IL NUOVO CIMENTO **47 C** (2024) 209
DOI 10.1393/ncc/i2024-24209-6

Colloquia: HADRON2023

Employing approximate symmetries for hidden pole extraction

A. Asokan(*)

Institute for Advanced Simulation and Institut für Kernphysik, Forschungszentrum Jülich D-52425 Jülich, Germany

received 21 December 2023

Summary. — Recent lattice analyses of the $D\pi$ scattering by Hadron Spectrum Collaboration (HadSpec) report only one pole in the D_0^* channel. This is in odds with the unitarised chiral perturbation theory analyses, which predict the $D_0^*(2300)$ as the interplay of two poles. We provide an explanation for this contradiction —the existence of a hidden pole. We further show that the hidden pole can be better extracted from the lattice data by imposing $SU(3)$ flavour constraints on the fitting amplitudes.

1. – Introduction

From unitarized chiral perturbation theory analyses, the structure of $D_0^*(2300)$ and $D_1(2430)$ can be understood as the interplay of two poles, corresponding to two scalar/axial-vector isospin doublet states with different $SU(3)$ flavor content [1-7]. These states emerge from non-perturbative dynamics of D mesons scattering off the Goldstone boson octet. This two-pole picture solves various problems that the experimental observation posed [6]. However, in the recent lattice analysis from HadSpec of $D\pi - D\eta - D_s\bar{K}$ coupled channel system at higher pion masses, only one pole was reported in the D_0^* channel, while it was not possible to extract reliable parameters of a second pole from the lattice data [8]. We here show that a higher pole does indeed exist in the lattice data albeit on hidden sheets and propose the use of $SU(3)$ flavour constraints to better capture its location.

2. – Analytic properties of the T-matrix

Except for branch cuts and poles the T-matrix is analytic over the whole complex plane. Right-hand cuts appear at every channel threshold, doubling the number of Riemann sheets. The sign of the imaginary part of the centre of mass momentum ($\mathrm{Im}(p_{cm})$) is used to label the sheets; see table 2 of ref. [9] for details. The physical sheet is the

(*) E-mail: a.asokan@fz-juelich.de

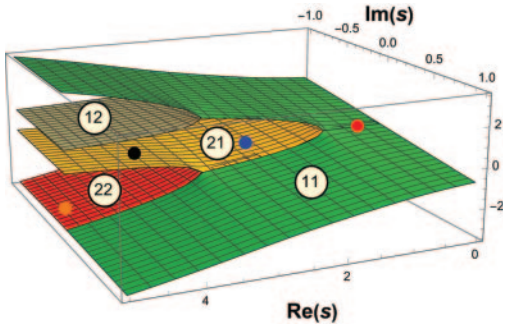

Fig. 1. – Illustration shows the sheet structure in case of a two-channel case. The pole shown in red corresponds to a bound state while blue, black and orange represent resonances.

Riemann sheet in which $\mathrm{Im}(p_{cm}) > 0$ for all channels. Depending on location, the poles correspond to bound states, virtual states or resonances. Hidden poles are resonance poles located on a sheet beyond the point at which it is connected directly to the physical sheet. Hence their effect on the amplitude can only be felt at the threshold, where the corresponding sheet is connected to the physical sheet. For example, the blue and orange points in fig. 1 are the poles which would produce a "conventional" resonance signal, while the black point would correspond to a hidden pole. And its effect on the amplitude would be felt at the second channel threshold. Poles located on the sheets closest to the physical sheet have the largest influence on the amplitude.

3. – Analysis of the lattice study amplitude

The analysis in ref. [8] was done by using a sizeable set of K-matrix parametrisations of the kind

$$K_{ij} = \frac{(g_i^{(0)} + g_i^{(1)} s)(g_j^{(0)} + g_j^{(1)} s)}{m^2 - s} + \gamma_{ij}^{(0)} + \gamma_{ij}^{(1)} s, \tag{1}$$

where i and j label the various channels, $g_i^{(n)}$, $\gamma_{ij}^{(n)}$ and m are real parameters determined from the fit to the lattice data. For the explicit form of the T-matrix see refs. [8,9]. A pion mass of $m_\pi = 391\,\mathrm{MeV}$ was used in the lattice study.

3˙1. *Pole search.* – In our labelling the closest sheets to the physical sheet above the respective thresholds are the sheets labelled RS211, RS221 and RS222. The lower pole in the studied channels appears as a bound state at the pion mass used in the lattice study and is accordingly located on sheet RS111 [8]; the same was seen in UChPT [5].

In our analysis we find in addition to the reported bound state pole, additional higher poles in sheets RS211, RS221 and RS222. These additional poles were found in almost all parametrisations employed by HadSpec we analysed. Figure 3 shows the locations of these higher poles in sheet RS221 from the HadSpec amplitude parametrisations and of the most prominent higher pole from the UChPT amplitude at the unphyical masses employed in the lattice study [5].

From fig. 3 we see that their locations do not scatter wildly between the parametrisations but show a significant correlation. All higher poles are seen to lie at higher energies

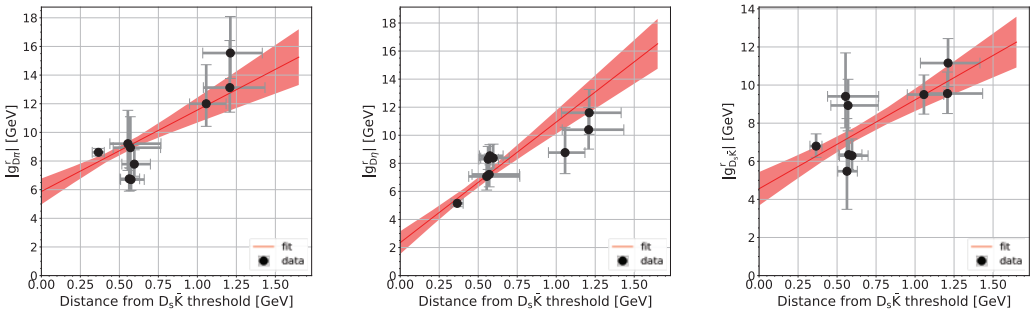

Fig. 2. – The distance of the real part of the pole from threshold *versus* the effective coupling of the pole to the $D\pi$ channel (left), $D\eta$ channel (middle) and $D_s\bar{K}$ channel (right). The red line shows the straight line fit. The red band encloses the 1σ uncertainty of the fit.

than the point where their respective Riemann sheet connects to the physical sheet, *i.e.*, they are located on hidden sheets. For example, the poles on RS221 lie beyond the $D_s\bar{K}$ threshold. They are shielded by RS222 and their effect can hardly be seen above the $D_s\bar{K}$ threshold. From the plot we see an increase in their widths as their distance from the threshold increases. We can see that the UChPT pole also lies in line with this correlation. To have an estimate of the effects of the poles at the respective threshold we plot the effective couplings from their residues to the different channels, with respect to the distance of the poles from the threshold. We quantified the distance as

$$\text{Dist} = M - M_{\text{thr}}, \tag{2}$$

where M_{thr} is the relevant threshold and M is the real part of the pole. Since the residues also drive the widths of the poles, eq. (2) was chosen to quantify the distance. Figure 2 shows the effective couplings *vs.* the distance plots. A straight line was fitted to extract the y intercept to use as an estimate of the effect of the poles at threshold. From the plots it is seen that this value is well constrained. We interpret this as the lattice data requires, in addition to the bound state pole, a second pole. The ill-constrained second pole locations are being balanced by their enhanced residue. This mechanism was also observed in the case of $f_0(980)$ and $a_0(980)$ [10]. This calls for a stronger constraint in the amplitude parametrisation to better confine the location of the higher hidden pole.

4. – $SU(3)$ flavour symmetry

We put forward a $SU(3)$ flavour constrained K-matrix to better capture the second pole location. Employing $SU(3)$ flavour symmetry is justified as we work with higher pion masses which leads to lower pion-kaon mass difference, moreover we are interested in the higher-mass range of the second pole. In these circumstances the leading $SU(3)$ breaking effects come from the loop functions.

The relation between the $SU(3)$ flavour basis and the isopin-symmetric particle basis is given by

$$\begin{pmatrix} |[\bar{3}]\rangle \\ |[6]\rangle \\ |[\overline{15}]\rangle \end{pmatrix} = U \begin{pmatrix} |D\pi\rangle \\ |D\eta\rangle \\ |D_s\bar{K}\rangle \end{pmatrix}; \quad U = \begin{pmatrix} -3/4 & -1/4 & -\sqrt{3/8} \\ \sqrt{3/8} & -\sqrt{3/8} & -1/2 \\ 1/4 & 3/4 & -\sqrt{3/8} \end{pmatrix}. \tag{3}$$

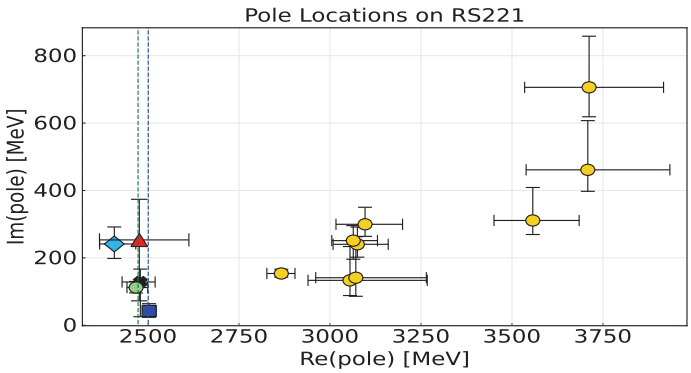

Fig. 3. – The location of poles on RS221 sheet. The x-axis and y-axis show the real and imaginary part of energy, respectively. The poles from the amplitude parametrizations employed in ref. [8] are shown in yellow. The pole from the UChPT amplitude [11] is shown in green [5].The higher pole locations extracted from the various fits are shown in red, cyan,black and blue. The vertical green and blue lines show the $D\eta$ and $D_s\bar{K}$ thresholds respectively.

The flavour constrained K-matrix is of the form

$$K = \left(\frac{g_{\bar{3}}^2}{m_{\bar{3}}^2 - s} + c_{\bar{3}}\right) C_{\bar{3}} + \left(\frac{g_6^2}{m_6^2 - s} + c_6\right) C_6 + c_{\overline{15}}\, C_{\overline{15}}, \tag{4}$$

where matrices $C_{\bar{3}}$, C_6 and $C_{\overline{15}}$ contain the $SU(3)$ symmetric coupling strengths and can be read off from eq. (3). For explicit forms see eqs. (20)–(22) in ref. [9]. The free parameters are g_α, c_α and m_α. Several fits with varying number of parameters were carried out to the energy levels in the lattice rest frame. The scheme introduced in ref. [12] was followed to perform the fits.

The higher pole locations extracted from fitting to the first four energy levels in the different lattice volumes at rest are shown in fig. 3. We see that the flavour constrained amplitude is successful in better capturing the hidden higher pole. The location of the lower bound state pole is consistent amongst all extractions. For a more in depth discussion on the quality of the fits and inclusion of higher lattice energy levels we refer the reader to ref. [9].

5. – Conclusion

A re-analysis of the K-matrix parametrisations provided in ref. [8] found, in addition to the reported bound state pole, additional poles on unphysical Riemann sheets in every amplitude. Though their locations vary greatly between parametrisations, their effects on the amplitudes were comparable in all parametrisations. We identify the origin of this as their location on hidden sheets. In such scenarios their effect on the amplitude becomes visible at threshold, and their distance from threshold can be balanced by an enhanced residue. To extract the higher pole from lattice data we propose an $SU(3)$ flavour constraint on the K-matrix. The flavour constrained amplitude is seen to be able to reproduce energy levels well and produce a pole at $D\eta$ and $D_s\bar{K}$ thresholds. It is interesting to obeserve that this pole is in fact consistent with that of the UChPT

amplitudes. Such a symmetry constrained amplitude maybe used in analysing other lattice data and also experimental data involving multiple channels.

* * *

I am very grateful to Christopher Thomas and David Wilson for very valuable discussions and for providing us with the results of ref. [8]. I thank all the co-authors of ref. [9] for their valuable input and for their contributions to the analysis done therein. This work is supported by the MKW NRW under the funding code NW21-024-A.

REFERENCES

[1] Kolomeitsev E. E. *et al.*, *Phys. Lett. B*, **582** (2004) 39, arXiv:hep-ph/0307133.
[2] Guo Feng-Kun *et al.*, *Phys. Lett. B*, **641** (2006) 278, arXiv:hep-ph/0603072.
[3] Guo Feng-Kun *et al.*, *Phys. Lett. B*, **647** (2007) 133, arXiv:hep-ph/0610008.
[4] Guo Feng-Kun *et al.*, *Eur. Phys. J. A*, **40** (2009) 171, arXiv:0901.1597 [hep-ph].
[5] Albaladejo Miguel *et al.*, *Phys. Lett. B*, **767** (2017) 465, arXiv:1610.06727 [hep-ph].
[6] Du Meng-Lin *et al.*, *Phys. Rev. D*, **98** (2018) 094018, arXiv:1712.07957 [hep-ph].
[7] Lutz Matthias F. M. *et al.*, *Phys. Rev. D*, **106** (2022) 114038, arXiv:2209.10601 [hep-ph].
[8] Moir Graham *et al.*, *JHEP*, **10** (2016) 011, arXiv:1607.07093 [hep-lat].
[9] Asokan Anuvind *et al.*, *Eur. Phys. J. C*, **83** (2023) 850, arXiv:2212.07856 [hep-ph].
[10] Baru V. *et al.*, *Eur. Phys. J. A*, **23** (2005) 523, arXiv:nucl-th/0410099.
[11] Liu Liuming *et al.*, *Phys. Rev. D*, **87** (2013) 014508, arXiv:1208.4535 [hep-lat].
[12] Döring M. *et al.*, *Eur. Phys. J. A*, **47** (2011) 139, arXiv:1107.3988 [hep-lat].